Received: 26 December 2019 | Revised: 14 April 2020 | Accepted: 22 April 2020

DOI: 10.1002/er.5550

RESEARCH ARTICLE

INTERNATIONAL JOURNAL OF ENERGY RESEARCH WILEY

Mechanical degradation of proton exchange membrane during assembly and running processes in proton exchange membrane fuel cells with metallic bipolar plates

Wenqing Liu[1] | Diankai Qiu[1] | Linfa Peng[1] | Peiyun Yi[1] | Xinmin Lai[1,2]

[1]State Key Laboratory of Mechanical System and Vibration, Shanghai Jiao Tong University, Shanghai, China

[2]Shanghai Key Laboratory of Digital Manufacture for Thin-Walled Structures, Shanghai Jiao Tong University, Shanghai, China

Correspondence
Xinmin Lai, Shanghai Key Laboratory of Digital Manufacture for Thin-walled Structures, Shanghai Jiao Tong University, Shanghai 200240, China.
Email: xmlai@sjtu.edu.cn

Funding information
National Key Research and Development Program of China, Grant/Award Number: 2017YFB0102803; National Natural Science Foundation of China, Grant/Award Number: 51705308

Summary

The mechanical degradation of the proton exchange membrane (PEM) is one of the main aspects affecting the lifetime of proton exchange membrane fuel cells (PEMFCs). It was observed in our previous study that the stress/strain distribution in the PEM of fuel cells with metallic bipolar plates (BPPs) is more complex, owing to manufacturing and assembly errors of the BPPs. The present study further concentrates on the stress/strain evolution in the membrane of fuel cells throughout the assembly and running processes by a finite element model. In membranes at the joint area between the gasket and gas diffusion layers, a serious stress concentration aggravated as the misalignment displacement increases. As for the membrane in reaction area, the plastic strain reaches highest level at the center of the groove after hygrothermal loading. The maximum stress is mainly relevant to the temperature and humidity and has little concern with the misalignment. The model and results of this study offer guidance regarding the design of PEMFC. Owing to the stress concentration, an additional protection should be set in the joint area, and the assembly error should be limited within 0.05 mm.

KEYWORDS

mechanical failure, membrane degradation, metallic bipolar plates, misalignment, relative humidity, temperature

1 | INTRODUCTION

The next-generation energy systems are significantly oriented by proton exchange membrane fuel cells (PEMFC) owing to their high-performance and zero carbon emissions.[1] However, commercial use of PEMFCs has been limited by the lifetime of the fuel cell systems.[2-4] The current durability objectives carried out by the U.S. Department of Energy is 5000 hour for transportation and 80 000 hour for medium-scale power stations by 2020.[5]

PEMFCs are composed of bipolar plates (BPPs), membrane electrodes assemblies (MEA), sealing gaskets, and two endplates used to compress the parts together. MEA is the core component in a fuel cell where electrochemical reaction occurs. During the running process of PEMFCs, proton exchange membrane (PEM) in the center of MEA plays an important role in the transport of protons and separation of hydrogen and oxygen. Any damage that occurs on the PEM will affect the cell reaction, reducing the performance and lifetime of the cell. According to previous studies, it has been found that the membrane itself is a major source of failure, including mechanical damage and chemical degradation.[6-8] Thus, the membrane must be enhanced in terms of both mechanical strength and chemical stability to extend the lifetime under severe internal operating conditions.[9,10]

Mechanical degradation is thought to cause infant mortality compared with progressive chemical degradation.[11-13] Studies describing a mechanical characterization of the failure in a membrane are available in the literature, which mainly investigates the failure mechanisms in reaction area and how the hygrothermal stresses influence such failures.[14] Experiment technique including accelerated degradation tests has been used on mechanical degradation.[15,16] For example, Sayadi et al[17] experimentally revealed the linear relationships among the hydrogen crossover rate, temperature, pressure, and relative humidity. Tang et al[18] found that the in-plane stress was the main factor rather than the stress in other terms, causing a membrane failure under hygrothermal conditions. Meanwhile, computational models were also used in degradation researches.[19-21] Kusoglu et al[22] conducted a material test on the original Nafion and PTFE enhanced membranes, and took the plastic factor into account, estimating the influence of the RH cycle on the membranes during the assembly and running operations using an finite element (FE) model. Lu et al[23] investigated the influence of the gas diffusion electrode (GDE) modulus and geometry of the reaction area on the stress distribution in PEMFC, and focused on the stress occurring in the reaction area. Uchiyama discovered a wrinkle deformation of an MEA and conducted a series of studies based on this development. They determined that cracks in the catalyst layer (CL) occur through buckling owing to the stresses during repeated humidity cycles, thereby causing the formation of pinholes in the membrane.[24]

In addition to the overall studies on the damage occurring in the reaction area, some researchers found another type of failure based on pinhole or crack in the joint area between the frame of MEA and GDE (the joint area in Figure 1). Li et al[25] and Wu et al[26] both found a sudden failure after a short period of accelerated stress test. It was notable that the open circuit voltage fell at the same instant in their studies. The sudden gas crossover rises and a quick performance degradation was considered to be caused by a fracture growth at the edge of frame. Ye et al[27] found a failure owing to shear stress occurred at the edge of the frame during the assembly process owing to the difference in softness of the membrane, although their study used a model that only considers the frame and membrane, and the material property was be linear, elastic, and constant.

Besides, current PEMFC BPP materials can be divided into two types: graphite BPPs and metal BPPs, and the distinction of BPP would influence the stress in the membrane. Thin metallic BPPs have been more widely used in passenger vehicles compared with graphite BPPs owing to its better performance in terms of mechanical strength, heat conduction, and relatively low cost for mass production.[28,29] However, current researchers usually focus on the electricity of graphite plates with rectangular shapes. Due to the characteristics of stamping process, metal BPPs usually have oblique angles in the reaction area whereas graphite BPPs have right angles. In addition, our previous study pointed out that the use of stamped thin metallic BPPs will cause unavoidable manufacturing and assembly errors.[30] We also found a dislocation of the BPPs will

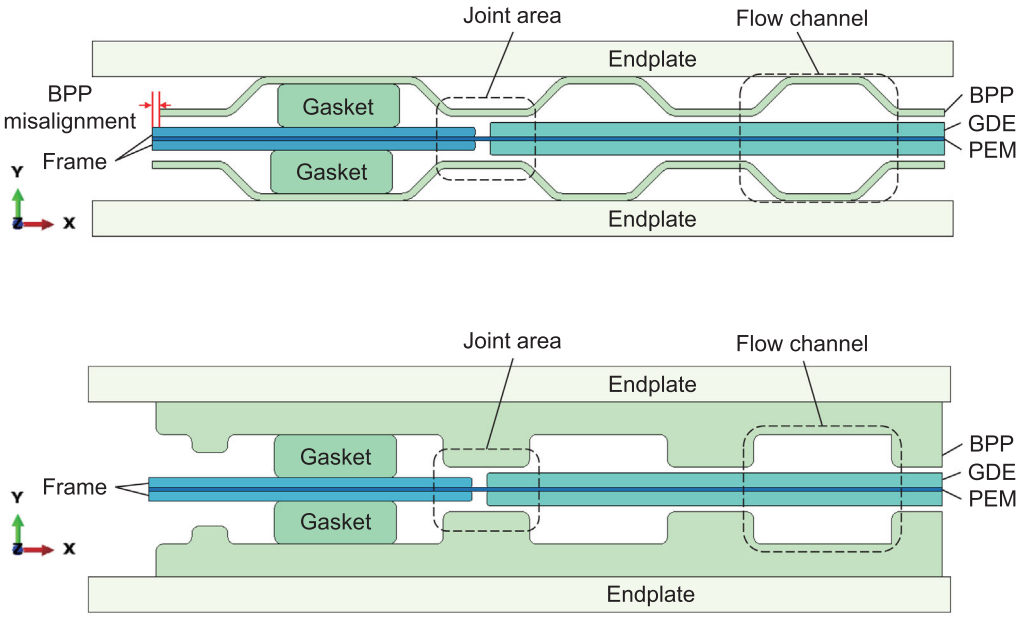

FIGURE 1 Numerical models of PEMFC: A, Metal bipolar with misalignment; B, graphite plates. PEMFC, proton exchange membrane fuel cell [Colour figure can be viewed at wileyonlinelibrary.com]

increase the stress and strain significantly, which means a failure may occur in the membrane earlier than the prediction made by previous studies.[31] These distinctions make it important to find the general rules of assessment for a fuel cell.

This study was conducted to clarify the understanding of the mechanical failure material influence on the difference in stress, as well as a membrane failure in both the reaction area and the joint area in the PEMFCs. It provides new insight into the mechanical failure of a membrane at multiple areas in a metal BPP PEMFC. The different influences on the mechanical failure of a PEMFC between metal and graphite BPPs were discussed. On this basis, the effects of a BPP misalignment caused by manufacturing and assembly errors of the metallic BPP on the mechanical degradation were thoroughly analyzed. This was followed by a failure analysis according to the stress and strain obtained.

2 | NUMERICAL MODEL

2.1 | Assumption

To simplify the calculation without significant influence in the accuracy, the numerical models used in this study apply the following presupposition:

(1) The CL is not considered in this analysis. The CL is extremely thin and is always considered a whole component within the GDE. In many other studies on membrane behaviors,[27,32,33] researchers usually integrate the CL into GDEs, and it shows little influence on the mechanical response.

(2) The main purpose of this study is to reveal the mechanical degradation regarding temperature and humidity changes. Thus chemical products are neglected during the analysis, and the chemical reaction is assumed only causing the heat generation in the fuel cell.

(3) To simplify the calculation process, the temperature and RH is assumed to change simultaneously in all components, and the membrane is the only component that swells during the hygrothermal process.

(4) All properties listed in Table 1 are isotropic and time-independent except the GDE material, meaning the viscosity and accumulation of plastic strain are not considered. Regarding the GDE layer, researchers have pointed out the anisotropy would influence the membrane stresses,[23,34,35] thus the anisotropy is considered in the model.

2.2 | Geometry and boundary conditions

Variations of stress and strain in the PEM during the whole life of a PEMFC is the focus of this study. The developed FE model based on the given data is shown in Figure 1. The geometry of the components such as the BPP and gaskets was based on the measured results. The frame was designed to be thinner than the GDE, to allow the GDE to have full contact with BPPs. During manufacturing processes of the MEA, five layers of components were hot-pressed. The initial misalignment of BPPs was set to 0.1 mm in our FE model (as shown in Figure 1A) and detailed data are listed in Table 5.

This simulation used a plane strain model to analyze the stress distribution. A type of flat element with a thickness of approximately 0.005 mm and relatively larger width was used to simulate the membrane because the thickness of membrane was extremely small (about 0.05 mm). The other parts were meshed according to their own dimensions, and some meshes may be refined in the region of the stress concentration. Two types of contact were considered among these components. General "surface-to-surface" contacts were used to describe a common touch behavior such as the contact between GDEs and BPPs. In addition, a bonded contact was used

TABLE 1 Datasheet on the material properties

Parts	Material	Young's modulus (MPa)	Poisson's ratio	Yield strength (MPa)	Expansion coefficient (K^{-1})
BPP	Stainless steel	197 000	0.3	290 000	16×10^{-6}
	Graphite	10 000	0.25	30	8.0×10^{-6}
GDE	Carbon paper	9000 (in-plane) 0.5 (through-plane)	0.09	–	-0.8×10^{-6}
PEM	Nafion® 212	See Table 2	0.24	See Table 3	122×10^{-6}
Frame	PEN	600	0.3	–	60×10^{-6}
Gasket	Silica gel	See Table 4	0.49	–	790×10^{-6}

Abbreviations: BPP, bipolar plate; PEM, proton exchange membrane; PEN, polyethylene naphthalate.

to describe the glued components, such as the frame and membrane. The assembly process was considered by fixing the bottom endplate and applying a displacement on the upper endplate. The model was symmetric to simplify the calculations.

The influence of a misalignment in the stack during the assembly and operating conditions was simulated by moving the upper BPP to the left once by 0.05 mm before the initial assembly process. Thereafter, the compression and hygrothermal processes were the same as the standard versions. The differences in the results were discussed in the following sections.

2.3 | Material and constitutive model

This study aims to analyze the influence of BPP materials and different misalignment displacements on the stress and strain distribution. One kind of metal BPPs is made of stainless steel and the other kind is made of graphite. The material used in the frame is polyethylene naphthalate.[27] And the mechanical behavior of these materials is considered linear-elastic during the analysis.[6,27,36]

In this FE analysis, the GDE undertook not only the compression from the BPPs, but also the shearing stress caused by a misalignment. From a previous study, GDE is a type of orthotropic material, then the anisotropic model was introduced to solve the large module difference in the in-plane and through-plane directions.[35] The gasket shows significant flexibility because it is manufactured from silicon rubber. The nonlinear stress-strain response is considered using a hyperelastic polynomial model according to our previous study.[37]

During the assembly and running procedures of a PEMFC, the influences of temperature and humidity are shown through both expansion and changes in mechanical property. For the membrane, experiments have proved that the mechanical property of membranes is nonlinear, as well as temperature and humidity dependent. To simplify the calculation, we used an isotropic elastic-plastic model.

In our numerical model, the total strain tensor of the membrane is considered to be composed of the elastic strain $\varepsilon_{ij}^{\mathrm{el}}$, plastic strain $\varepsilon_{ij}^{\mathrm{pl}}$, and temperature and swelling induced strains $\varepsilon_{ij}^{\mathrm{th}}$ and $\varepsilon_{ij}^{\mathrm{sw}}$:

$$\varepsilon_{ij} = \varepsilon_{ij}^{\mathrm{el}} + \varepsilon_{ij}^{\mathrm{pl}} + \varepsilon_{ij}^{\mathrm{th}} + \varepsilon_{ij}^{\mathrm{sw}}. \tag{1}$$

Thermal strain generated at the current temperature T, with respect to the reference temperature T_0 (25°C), is

$$\varepsilon_{ij}^{\mathrm{th}} = \alpha(T - T_0)\delta_{ij} \text{ with } \delta_{ij} = \begin{cases} 1(i=j) \\ 0(i\neq j) \end{cases}, \tag{2}$$

where α is the thermal expansion coefficient and δ_{ij} is the Kronecker delta.

The isotropic swelling strain is shown as follows:

$$\varepsilon_{ij}^{\mathrm{sw}} = \beta(\mathrm{RH} - \mathrm{RH}_0)\delta_{ij} \text{ with } \delta_{ij} = \begin{cases} 1(i=j) \\ 0(i\neq j) \end{cases}, \tag{3}$$

where β is the swelling expansion coefficient, similar to α in the thermal expansion, and RH_0 is the reference value of RH.

Regarding elastic strain, Hooke's law gives the relationship between stress and strain:

$$\sigma_{ij} = \frac{E}{(1+\nu)(1-2\nu)}\left[\nu\varepsilon_{kk}^{\mathrm{el}} + (1-2\nu)\varepsilon_{ij}^{\mathrm{el}}\right], \tag{4}$$

where σ_{ij} is the true stress of the material, E is the Young's modulus, ν is the Poisson's ratio, and $\varepsilon_{kk}^{e} = \varepsilon_{11}^{e} + \varepsilon_{22}^{e} + \varepsilon_{33}^{e}$, the Young's modulus can be obtained from the Table 2.[6]

As shown in Figure 2, the elastoplastic stress-strain curve is assumed to be a piecewise function with three pieces. The plastic strain is assumed to be zero at first, and two additional stress points are added at σ_{ij}^{1} (T,H; $\varepsilon_{ij}^{\mathrm{pl}} = 0.05$), and σ_{ij}^{2} (T,H; $\varepsilon_{ij}^{\mathrm{pl}} = 0.25$). Detailed value of yield stresses is listed in Table 3. The stress-strain response at other temperature and humidity were calculated by linear interpolation based on the available stress-strain curves of the material (Tables 2 and 3).

2.4 | Assembly and running loading

The simulated assembly and loading processes are conducted in two steps as follows:

Over the entire life of PEMFC, the assembly comes first. In the assembly process, all the components are placed in the preset order. The upper endplate is then pushed, and the components are compressed to a desirable compression of 20%. The endplates are considered motionless at all times after the assembly.

TABLE 2 Young's modulus of the membrane at various temperature and humidity

	Relative humidity (%)			
	30	**50**	**70**	**90**
$T = 25°C$	197	192	132	121
$T = 45°C$	161	137	103	70
$T = 65°C$	148	117	92	63
$T = 85°C$	121	85	59	46

The second step is imposing hygrothermal loading on the components. During our simulation, the loading is applied by improving the temperature and humidity simultaneously (25°C and 30% RH to 85°C and 90% RH).[24,38] The temperature leads to a heat expansion in all components as determined through their own heat expansion coefficient, and the humidity only influences the swelling of membrane. As mentioned in Section 2.3, changing in temperature and humidity also influenced the yield strength of membranes. The gradients of temperature and humidity are not considered under the assumption that the temperature and RH change simultaneously in all components.

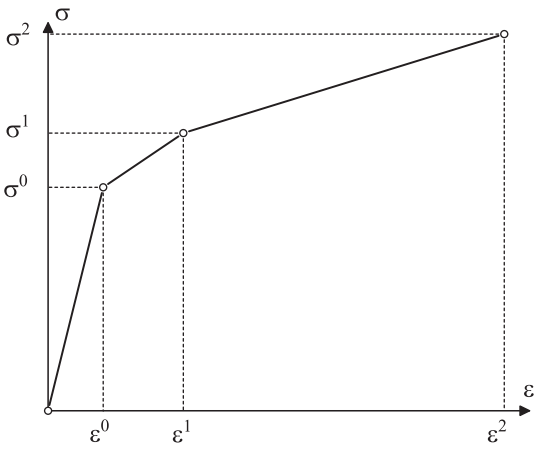

FIGURE 2 Equivalent plastic strain in the PEM at the joint area after hygrothermal loading. PEM, proton exchange membrane

TABLE 3 Yield strength of the membrane at various temperature and humidity

		Relative humidity (%)			
		30	50	70	90
$\varepsilon^{pl} = 0$	$T = 25°C$	6.76	6.51	5.66	4.20
	$T = 45°C$	5.67	5.21	5.01	3.32
	$T = 65°C$	5.14	4.58	4.16	2.98
	$T = 85°C$	3.61	3.44	3.08	2.20
$\varepsilon^{pl} = 0.05$	$T = 25°C$	7.16	6.61	6.22	5.11
	$T = 45°C$	5.70	5.72	5.43	3.69
	$T = 65°C$	5.30	4.77	4.36	3.33
	$T = 85°C$	4.16	3.62	3.16	2.26
$\varepsilon^{pl} = 0.25$	$T = 25°C$	9.71	9.26	8.65	8.88
	$T = 45°C$	7.31	7.34	7.48	6.18
	$T = 65°C$	6.55	5.92	5.73	5.78
	$T = 85°C$	5.04	4.28	4.22	4.31

3 | MODEL VALIDATION

In order to validate the FE method in this study, the simulated compression behavior of the membrane were compared with the results of Kusoglu et al's research. In their study, a single unit of a PEMFC model was built to investigate the stress distribution in the membrane when hygrothermal conditions changed.[6] The finite element model is shown in Figure 3A. The in-plane stresses in the membrane are compared because of its significant influence on the mechanical degradation of the membrane.

During the hygrothermal cycles, the environment gradually changed from the initial (30% RH and 20°C) to the hygrothermal loading condition (95% RH and 85°C) according to their article.[6] Figure 3B shows the difference in the consequent in-plane stresses on the surface of membrane between the two models. Both models show the same tendency and quantity of the in-plane stress. The maximum difference between two methods were 0.75 MPa for the left side and 1.23 MPa for the right side, which is 18.9% and 15.3%. The small differences are caused by the difference on GDE property setting, which is isotropic in Kusoglu's model and anisotropic in this article.[6] As the overall order of the calculation is 10 MPa, the results indicate that the model introduced in Section 2.3 are sufficiently accessible.

4 | INFLUENCE OF BPP TYPES ON THE MEMBRANE STRESS

4.1 | Shape difference

Owing to the strong toughness and ductility of material, metal BPPs are stamped into sections of slices, whereas graphite BPPs are usually manufactured through milling, extrusion, or compression molding. The round corner of the reaction area in the metal BPPs is usually greater than that of graphite BPPs because of the manufacturing techniques. Clearly, the differences in material property and manufacturing method lead to different shapes and therefore different distribution of stress. This distinction

TABLE 4 Datasheet on silicon property of gasket

Parameters	D_1	C_{10}	C_{20}	C_{01}	C_{11}	C_{02}
Value	0.30	4.78	64.35	−4.72	−149.69	86.53

TABLE 5 Dimensions in FE model

Parameters	Value (mm)	
BPP	Thickness	0.1
	Channel height	0.4
	reaction area width	1.0
	Sealing channel width	2.2
Gasket thickness		0.60
Frame thickness		0.10
GDE thickness		0.20
Nafion® membrane thickness		0.05
Joint width		0.10

Abbreviation: BPP, bipolar plate.

makes it important to find the general rules of assessment in the fuel cell.[39]

The shape differences were studied using two models of same metal material but with different structure as shown in Figure 1. The distribution of the von Mises stress, in-plane stress (S11), and through-plane stress (S22) of the PEM at the joint area after entire loadings is shown in Figure 4. The stamped BPP showed a significant difference compared with milled BPP. From the stress distribution, a greater through-plane stress value at 4.15 MPa was observed in the model with milled BPPs, which was only 3.70 MPa in the model using stamped BPP. The reason for this is the slight deformation of the stamped BPP during compression causing a greater actual distance between the GDEs and the smaller deformation of the membrane. In Khorasany's research on mechanical failure, the SWT model was used to study the failure of membrane. The

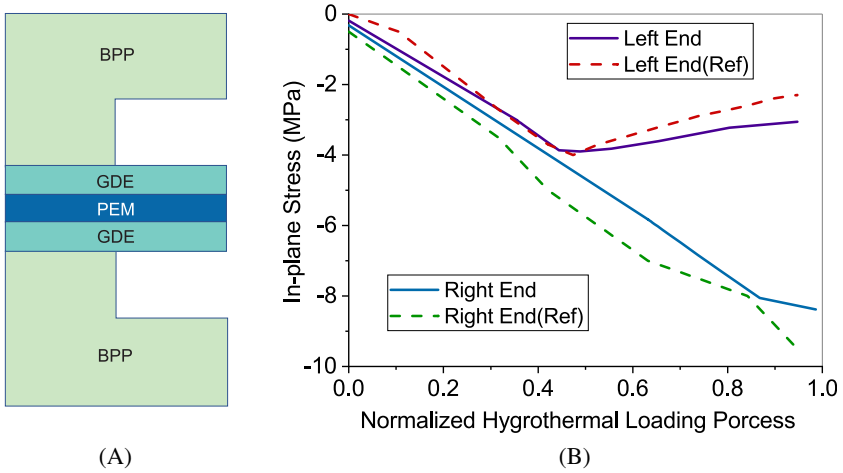

FIGURE 3 A, Schematic of the FE model for validation (the dimensions are not in proportion); B, the evolution of in-plane stress on the selected points during the hygrothermal loading process [Colour figure can be viewed at wileyonlinelibrary.com]

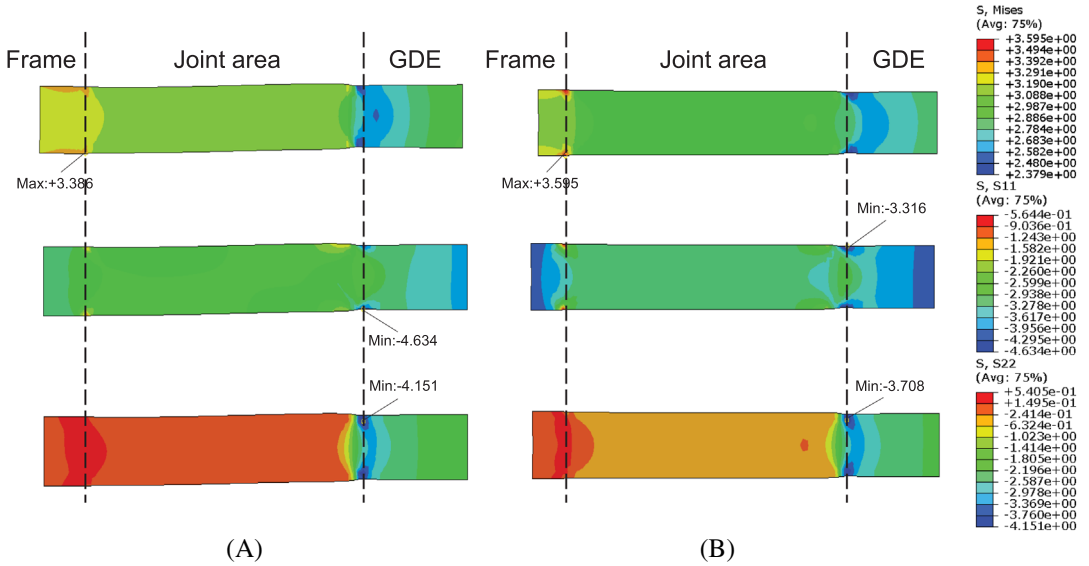

FIGURE 4 Stresses at the joint area: A, Metal milled BPP with rectangular reaction area edge; (B) metal stamped BPP with oblique reaction area edge. BPP, bipolar plate [Colour figure can be viewed at wileyonlinelibrary.com]

model indicates that failure is more related to the in-plane stress.[40] With regard to the in-plane stress (S11), the maximum in-plane stress reached 3.32 MPa whereas the maximum in-plane stress with a milled BPP was 4.63 MPa. In addition, the in-plane stress changed faster near the edge of each region with metal stamped BPP. This distinction is due to the bigger round of metal stamped BPP, which also reduced the stress concentration.

4.2 | Material features

The BPPs of a PEMFC have been through a long development period, and to date they are mainly based on two types of material. The first type is BPPs made of carbon-based material, including graphite, flexible graphite, C-C composite, or carbon-polymer composite.[41] The other type is the coated metal BPP, which have a greater stiffness than graphite ones.[42]

To explore the influence of BPP material, two types of material model were used in the analysis. Both models were set to the shape shown in Figure 1B. After clamping and hygrothermal loading, the von Mises, in-plane, and through-plane stresses at the joint area are list as shown in Figure 5.

As shown in first row of Figure 5, the von Mises stress occurred at only a 2.3% difference between the graphite and metal BPPs. However, the in-plane stress in the membrane of fuel cell using metal BPP was 4.63 MPa, much greater than a stress of 3.87 MPa with graphite BPP. The results also shows that the von Mises criterion is not enough for a detailed analysis of the membrane fatigue because it reflects a combined influence of three kinds of stresses, and the in-plane stress cannot be determined, which is the factor that counts.

5 | STRESS AND STRAIN IN THE MEMBRANE

The simulation of the in situ mechanical behavior was conducted with the above FE model in the joint area and reaction areas. To identify the region that determines the lifetime of the PEM, the stress distributions in the joint region and the reaction area during all processes were researched separately.

5.1 | Stress distribution in the joint area

The distribution of the von Mises stress, in-plane stress, and through-plane stress of the PEM at the joint area after entire loadings is shown in Figure 6.

A detailed stress analysis in the joint area during the clamping process has been previously conducted by our group.[30] In this study, GDE was first pushed onto the frame and membrane during the assembly process, constraining the in-plane movement of the other parts of the MEA. Figure 6 shows that during the hygrothermal process, the thermal expansion and swelling of the membrane were heavier than the other parts, pushing the stress concentration point right. The induced in-plane stress of 3.32 MPa can be observed in Figure 6. In particular, stress concentration occurred after hygrothermal loading, the in-plane stress grew from 0.7 to 3.32 MPa, which means that in-plane stress on the membrane in the joint area is crucial.

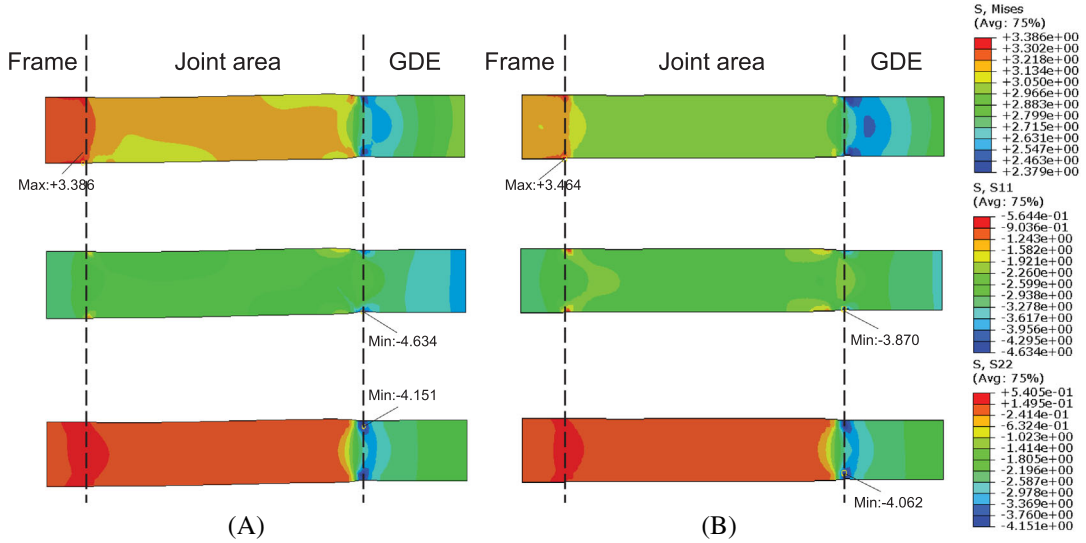

FIGURE 5 Stresses at the joint area in two types of BPP materials: A, Metal BPP; B, graphite BPP. BPP, bipolar plate [Colour figure can be viewed at wileyonlinelibrary.com]

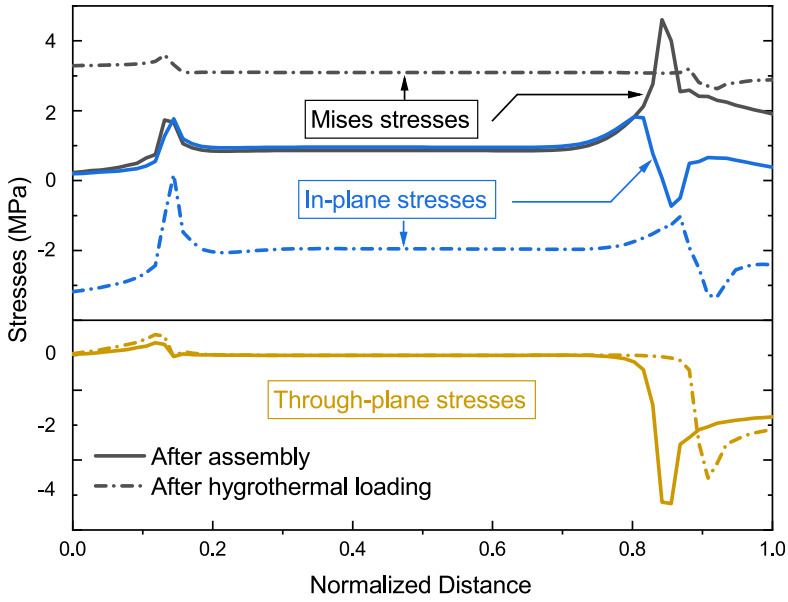

FIGURE 6 Stress distribution in the joint area [Colour figure can be viewed at wileyonlinelibrary.com]

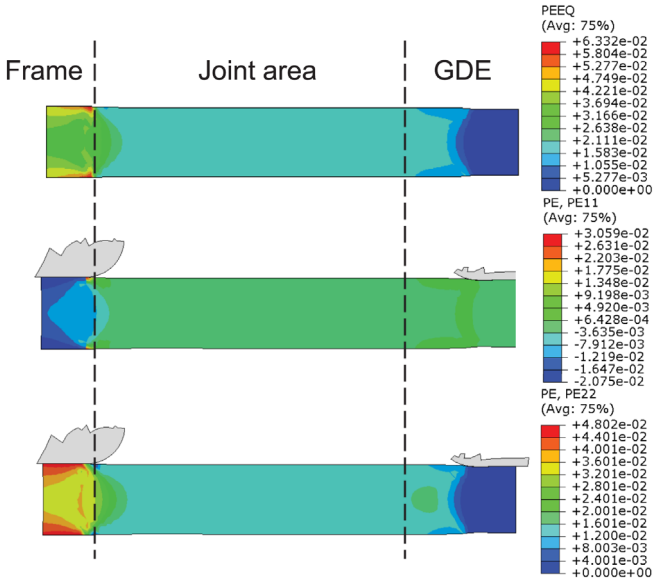

FIGURE 7 Equivalent plastic strain in the PEM at the joint area after hygrothermal loading. PEM, proton exchange membrane [Colour figure can be viewed at wileyonlinelibrary.com]

However, Figure 6 also shows the maximum von Mises stress at the final status decreased to 3.60 from 4.78 MPa in initial status. This phenomenon is in accordance with the heat and moisture softening effect of the membrane raised by Khorasany et al.[40]

As shown in Figure 7, by focusing on the plastic strain in the membrane, it can be seen that the frame constraints limited the membrane from expanding in the *x*-direction, and caused a large effective plastic strain (PEEQ) on the left side of the joint, which reveals a plastic deformation near the frame. After recovering from high hygrothermal conditions, the membrane would suffer from the remaining residual stress. In addition, this residual stress in the membrane could accumulate with the iterative cycling RH and temperature during the running process, leading to a mechanical failure. In general, the maximum plastic strain occurred between the frame and the edge of GDEs, which was just the fragile area for degradation during the running process.[30]

5.2 | Stress distribution in the channel

The stress/strain variation in the channel after assembly and hygrothermal loading is shown by Figure 8. Figure 8B shows that during the assembly process, in-plane stress S11 remained at less than 0.5 MPa within the whole channel, and through-plane stress S22 varied from 1.5 MPa under the ridge to zero at the channel center, which means that the main effect in assembly process is compression in *y*-direction of Figure 1.

During the hygrothermal process, the thermal expansion and swelling of the membrane were heavier than those in the other parts. A higher stress occurred in the membrane near the channel edges, which would significantly strengthen the in-plane stresses. From Figure 8C, S22 maintained the same level during the hygrothermal process, whereas S11 increased significantly within the entire region. The combination of increased stresses made the maximum von Mises stress increase from 0.5 to 3.33 MPa, which may create fatigue in the reaction area after numerous cycles. However, it should be noted that the location where the maximum von Mises stress occurred moved from the ridge to the groove. The in-plane stress after the hygrothermal loading was 3.3 to 4.68 MPa, and became the

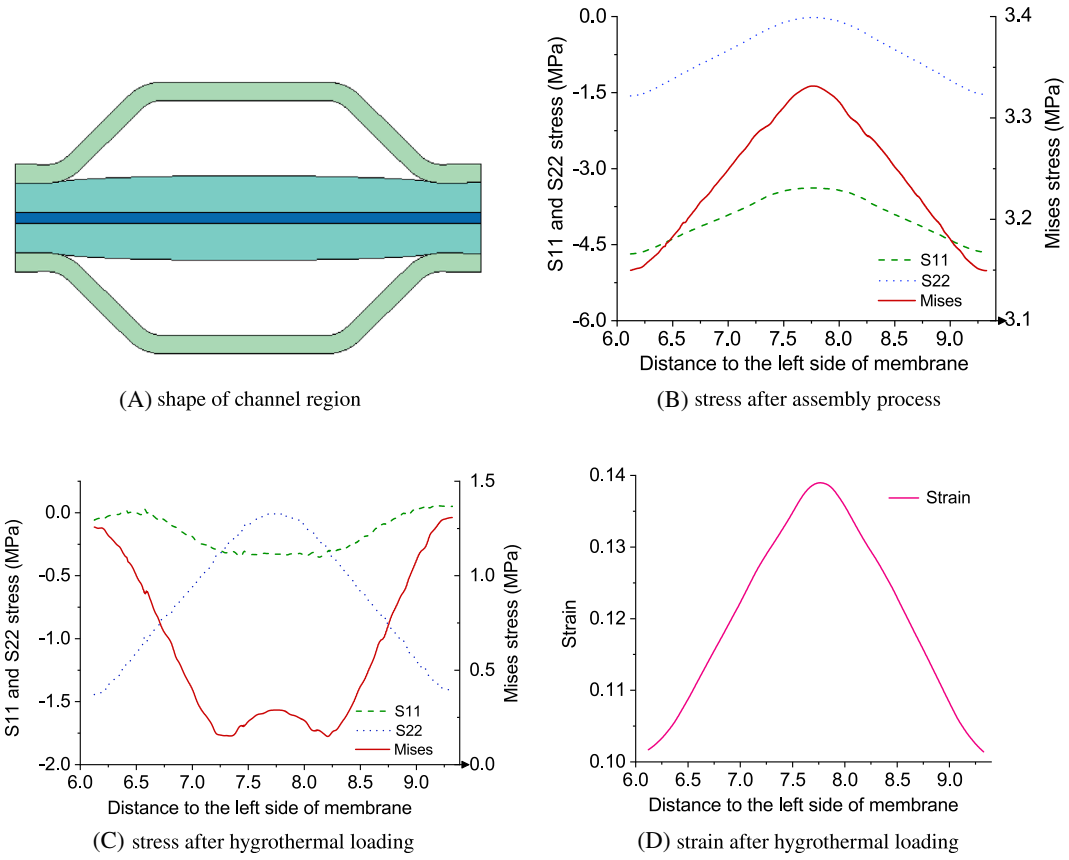

(A) shape of channel region (B) stress after assembly process

(C) stress after hygrothermal loading (D) strain after hygrothermal loading

FIGURE 8 Stress and strain distribution in the channel [Colour figure can be viewed at wileyonlinelibrary.com]

main factor causing a failure in the reaction area region. In particular, Figure 8C,D shows that both the in-plane and through-plane stress did not come to a maximum value at the groove center, whereas the von Mises stress and strain reached the maximum levels in the groove center. This made the groove center to be most plausible place of fatigue within the channel after hydrothermal cycles.

6 | EFFECTS OF MISALIGNMENT

The analysis reveals that the membrane experiences stress changes throughout the entire lifetime in both the joint area and the reaction area. Due to the manufacturing characteristics, the misalignment of metallic BPPs is unavoidable in the stack. In this section, the effects of the misalignment on the membrane degradation in these weak areas are discussed.

6.1 | Effects of misalignment in the joint area

Change in the stress from the assembly process to the hygrothermal process is mainly discussed in this section. In addition, the amplitude of stress is also a main factor affecting the durability of the membrane.[40] Thus, we will focus on the maximum value and the amplitudes of the in-plane stresses in the hygrothermal processes.

Figure 9A shows a typical distribution of the in-plane stress at the joint area when a misalignment occurs. Four points are selected to analyze the influence of a misalignment on the membrane stress. It can be seen that, owing to the expansion arising from the assembly, the severer bending makes the maximum in-plane stress on points 2 and 3 grow as the misalignment increases, which means that the misalignment mainly influences the stretching stress at the joint area.

Concerning the amplitude of in-plane stress during the hygrothermal loading process, points 2 and 3 also show sensitivity to the misalignment distance. An increase in the misalignment will produce stress ascending in the stretching area at the joint. Thus, more attention should be paid to the stress at points 2 and 3 during the entire process. From Curtin et al's study on PEM failure,[14] the stress amplitude should be less than 3.0 MPa. On Figure 9D, we can see that the amplitude of stress variation attained 3.0 MPa at a misalignment of 0.05 mm. Therefore, assembly error should be limited within 0.05 mm to satisfy the lifetime demand.

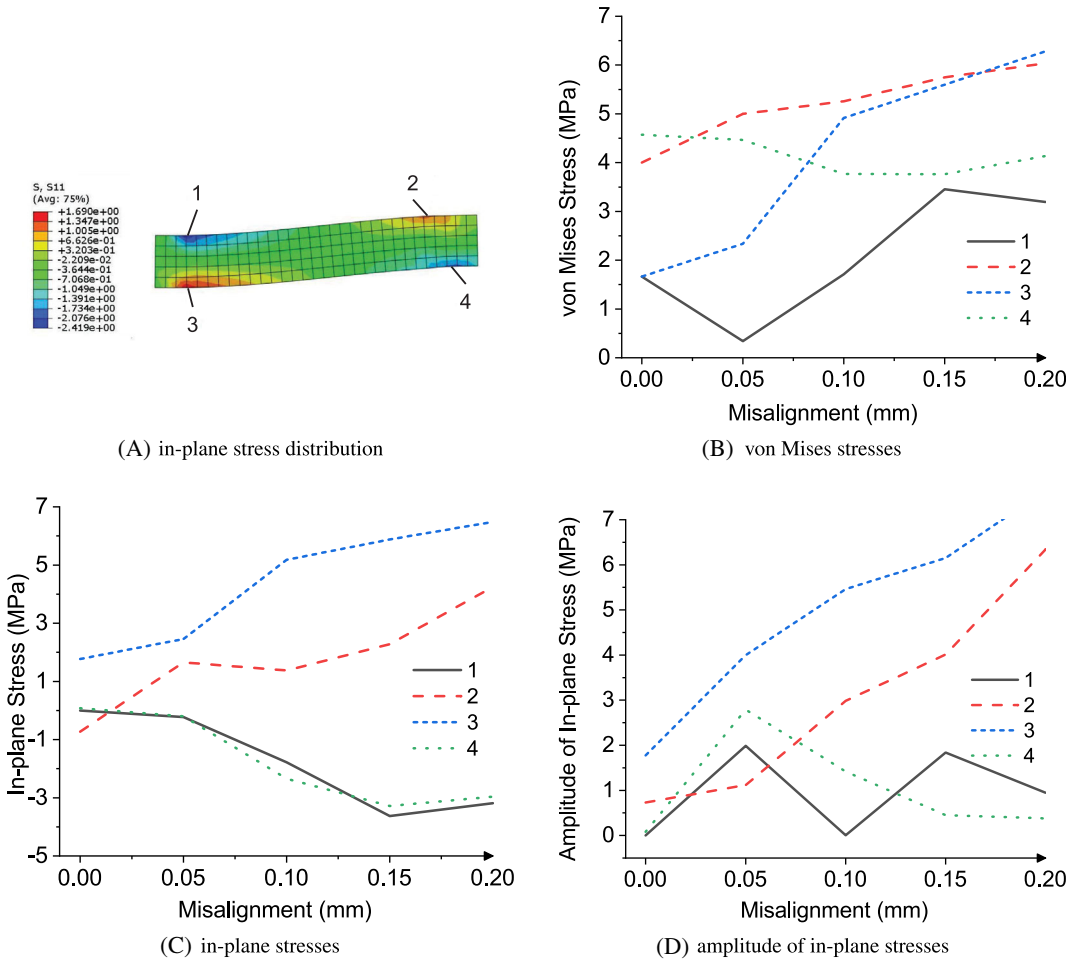

(A) in-plane stress distribution (B) von Mises stresses

(C) in-plane stresses (D) amplitude of in-plane stresses

FIGURE 9 Stress on the membrane at the joint area after hygrothermal loading [Colour figure can be viewed at wileyonlinelibrary.com]

6.2 | Effects of misalignment in the reaction area

This section is mainly discussing the effect of BPP misalignment on the stress and strain in the reaction area. The maximum in-plane stress after the hygrothermal process occurred at the center of the ridge, but the membrane in the channel area suffered from a larger equivalent plastic strain owing to the stretching of the compressed membrane (Figure 10A,B). Figure 10C shows the stress and its variation after hygrothermal loading, where it can be seen that the amplitude of stress in the channel was less than 0.1% in direct proportion to the value of the BPP misalignment. This indicates that a misalignment does not significantly influence the dimension of the membrane during the hygrothermal process in this area, and more attention should be paid to the expanding and swelling from the changes in the temperature and water content during hygrothermal loading.

From the fatigue studies by Christopher et al's, the lifetime of membrane is mainly influenced by the values of stress and amplitudes of strain.[38,43] The following analysis will focus on the change in plastic strain during the hygrothermal process.

The strain of the PEM is elastic strain through compression after assembly. When the fuel cell starts running, the temperature and humidity increase, leading to an expansion in the reaction area. A portion of expansion induced by the heat and hydration will become plastic strain that accumulates along with the hydrothermal loading. As shown in Figure 10D, the final equivalent plastic strain is approximately 5.8% at the groove and 2.2% under the ridge. Heat and moisture are thought to be the main sources of such change. Considering the in-plane stress mentioned in Section 5.2, as well as a larger plastic strain at the center of the groove under higher temperature and relative humidity, the center of the channel should be paid more attention to in a fatigue analysis within the reaction region.

In particular, both the stress and strain responses of the membrane in the channel are not related to the misalignment errors. This insensitivity to a misalignment

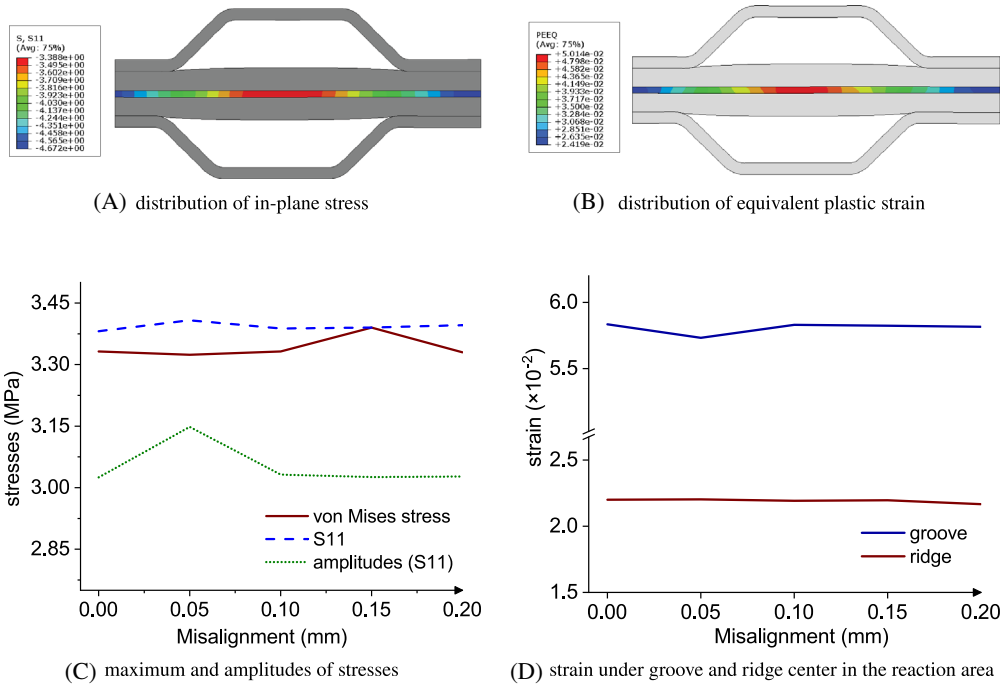

(A) distribution of in-plane stress

(B) distribution of equivalent plastic strain

(C) maximum and amplitudes of stresses

(D) strain under groove and ridge center in the reaction area

FIGURE 10 Stress and strain after hygrothermal process [Colour figure can be viewed at wileyonlinelibrary.com]

means that the main reason for a stress increase in reaction region is not the misalignment, but related more to the procedure itself, such as the temperature and humidity.

7 | CONCLUSION

Mechanical degradation in the PEM caused by a stress/strain variation is one of the crucial reasons for the failure of the fuel cells.[44] In this study, a PEMFC model was built to explore the difference in a metallic BPP PEMFC from a graphite version, and the membrane stress evolution was discussed in the joint area and reaction area in the entire process. The results indicate that fuel cells with metallic BPPs suffer from a smaller stress concentration than graphite versions owing to a difference in shape caused by the manufacturing approach. Moreover, the techniques of stamping in a metal BPP lead to unavoidable assembly errors in the PEMFC products. It is necessary to study how these errors affect the stress/strain distribution on the PEM.

Further analysis indicates that within the joint area, a stress/strain concentration is generated owing to a small bending near the compressed gasket by the force exerted during the assembly process. In the presence of assembly errors, a stress concentration will occur in the membrane at the gasket edge. By increasing the displacement of the misalignment, the concentration stress rises; the amplitude of stress during the hygrothermal procedure also becomes larger. The assembly error should be limited within 0.05 mm to control the stress range, and satisfy the lifetime demand.

Moreover, in the reaction area of a membrane, the maximum the von Mises stress occur under the ridge after assembly. After hygrothermal loading, the through-plane stress stays the same, and the maximum in-plane stress occurs under the ridge owing to the corresponding swelling. However, considering the failure process, both the von Mises stress and equivalent plastic strain attain the highest values at the center of the groove, indicating that a failure at the center of channel should first be considered in the reaction area. In addition, both the value and amplitude of the stress are insensitive to the misalignment. The results suggest that more attention should be paid to the temperature and water content rather than a misalignment when considering the mechanical degradation in the reaction area.

This study provides new insight into the mechanical failure of a membrane at multiple areas in a PEMFC. The different influences on the mechanical failure of a PEMFC between metal and graphite BPPs were discussed. On this basis, the effects of BPP misalignment caused by manufacturing and assembly errors of the metallic BPP on the mechanical degradation were thoroughly analyzed. The assembly error should be limited within 0.05 mm to satisfy the lifetime demand. However, only the first hygrothermal increase was discussed, and the effect of plastic strain accumulation was not considered in the analysis. During the entire lifetime, cyclic hygrothermal loading will cause an accumulation of plastic strain, the effects of which will be further studied.

ACKNOWLEDGEMENTS

This study was supported by the National Natural Science Foundation of China (Grant No. 51705308) and National Key Research and Development Program of China (2017YFB0102803).

ORCID

Wenqing Liu https://orcid.org/0000-0001-9035-7094

REFERENCES

1. Chang H, Duan C, Xu X, Pei H, Shu S, Tu Z. Technical performance analysis of a micro-combined cooling, heating and power system based on solar energy and high temperature PEMFC. *Int J Hydrogen Energy*. 2019;44(38):21080-21089.
2. Wilberforce T, El-Hassan Z, Khatib FN, et al. Developments of electric cars and fuel cell hydrogen electric cars. *Int J Hydrogen Energy*. 2017;42(40):25695-25734.
3. Dincer I. Environmental and sustainability aspects of hydrogen and fuel cell systems. *Int J Energy Res*. 2007;31(1):29-55.
4. Beuscher U, Cleghorn SJ, Johnson WB. Challenges for PEM fuel cell membranes. *Int J Energy Res*. 2005;29(12):1103-1112.
5. US DOE. Fuel Cell Technologies Office Multi-Year Research, Development, and Demonstration Plan. Technical Report, US Department of Energy; Washington, DC; 2016.
6. Kusoglu A, Karlsson AM, Santare MH, Cleghorn S, Johnson WB. Mechanical behavior of fuel cell membranes under humidity cycles and effect of swelling anisotropy on the fatigue stresses. *J Power Sources*. 2007;170(2):345-358.
7. Xie J, Wood DL, Wayne DM, Zawodzinski TA, Atanassov P, Borup RL. Durability of PEFCs at high humidity conditions. *J Electrochem Soc*. 2005;152(1):A104-A113.
8. Jiao K, Ni M. Challenges and opportunities in modelling of proton exchange membrane fuel cells (PEMFC). *Int J Energy Res*. 2017;41:1793-1797.
9. Chen B, Wang J, Yang T, et al. Mitigation studies of carbon corrosion by optimizing the opening size of the cathode outlet in a proton exchange membrane fuel cell with dead-ended anode. *Energ Conver Manage*. 2016;119:60-66.
10. Barbir F, Yazici S. Status and development of PEM fuel cell technology. *Int J Energy Res*. 2008;32(5):369-378.
11. Kundu S, Fowler M, Simon L, Grot S. Morphological features (defects) in fuel cell membrane electrode assemblies. *J Power Sources*. 2006;157(2):650-656.
12. Crum M, Liu W. Effective testing matrix for studying membrane durability in PEM fuel cells: part 2. Mechanical durability and combined mechanical and chemical durability. *ECS Transactions*. 2006;3(1):541.
13. Stanic V, Hoberecht M. Mechanism of pinhole formation in membrane electrode assemblies for PEM fuel cells. *ECS Proc Vol*. 2004;2004:391-401.
14. Curtin DE, Lousenberg RD, Henry TJ, Tangeman PC, Tisack ME. Advanced materials for improved PEMFC performance and life. *J Power Sources*. 2004;131(1–2):41-48.
15. Jao TC, Jung GB, Ke ST, Chi PH, Chan SH. Diagnosis of PTFE-Nafion MEA degradation modes by an accelerated degradation technique. *Int J Energy Res*. 2011;35(14):1274-1283.
16. Jao TC, Jung GB, Ke ST, Chi PH, Su A. In situ analysis of MEA performance under accelerated degradation testing. *Int J Energy Res*. 2011;35(14):1284-1290.
17. Sayadi P, Rowshanzamir S, Parnian MJ. Study of hydrogen crossover and proton conductivity of self-humidifying nanocomposite proton exchange membrane based on sulfonated poly (ether ether ketone). *Energy*. 2016;94:292-303.
18. Tang Y, Santare MH, Karlsson AM, Cleghorn S, Johnson WB. Stresses in proton exchange membranes due to hydration-dehydration cycles. Paper presented at: American Society of Mechanical Engineers Digital Collection; 2005;207-213.
19. Kim Y. Study on the effect of humidity and stoichiometry on the water saturation of PEM fuel cells. *Int J Energy Res*. 2012;36(4):509-522.
20. Jung CY, Kim WJ, Yoon CS, Kim DH, Yi SC. Computational modeling of proton exchange membrane fuel cells including gas-crossover behavior. *Int J Energy Res*. 2013;37(15):1981-1991.
21. Ahmadi P, Kjeang E. Realistic simulation of fuel economy and life cycle metrics for hydrogen fuel cell vehicles. *Int J Energy Res*. 2017;41(5):714-727.
22. Kusoglu A, Karlsson AM, Santare MH, Cleghorn S, Johnson WB. Mechanical response of fuel cell membranes subjected to a hygro-thermal cycle. *J Power Sources*. 2006;161(2):987-996.
23. Lu Z, Kim C, Karlsson AM, Cross JC III, Santare MH. Effect of gas diffusion layer modulus and land–groove geometry on membrane stresses in proton exchange membrane fuel cells. *J Power Sources*. 2011;196(10):4646-4654.
24. Uchiyama T, Kato M, Yoshida T. Buckling deformation of polymer electrolyte membrane and membrane electrode assembly under humidity cycles. *J Power Sources*. 2012;206:37-46.
25. Li B, Kim YS, Mukundan R, et al. Mixed hydrocarbon/fluoropolymer membrane/ionomer MEAs for durablity studies. *ECS Trans*. 2010;33(1):913-924.
26. Wu B, Zhao M, Shi W, et al. The degradation study of Nafion/PTFE composite membrane in PEM fuel cell under accelerated stress tests. *Int J Hydrogen Energy*. 2014;39(26):14381-14390.
27. Ye D, Zhan Z, Lee Y, Tu Z, Zhang Y, Pan M. Effects of frame materials and structures on stress concentration of membrane electrode assembly of PEMFCs. *Fuel Cells*. 2013;13(6):1205-1212.
28. Hermann A, Chaudhuri T, Spagnol P. Bipolar plates for PEM fuel cells: a review. *Int J Hydrogen Energy*. 2005;30(12):1297-1302.
29. Qiu D, Yi P, Peng L, Lai X. Study on shape error effect of metallic bipolar plate on the GDL contact pressure distribution in proton exchange membrane fuel cell. *Int J Hydrogen Energy*. 2013;38(16):6762-6772.
30. Qiu D, Peng L, Liang P, Yi P, Lai X. Mechanical degradation of proton exchange membrane along the MEA frame in proton exchange membrane fuel cells. *Energy*. 2018;165:210-222.
31. Qiu D, Peng L, Lai X, Ni M, Lehnert W. Mechanical failure and mitigation strategies for the membrane in a proton exchange membrane fuel cell. *Renew Sustain Energy Rev*. 2019;113:109289.
32. Omrani R, Seif Mohammadi S, Mafinejad Y, Paul B, Islam R, Shabani B. PEMFC purging at low operating temperatures: an experimental approach. *Int J Energy Res*. 2019;43(13):7496-7507.
33. Nanadegani FS, Lay EN, Sunden B. Effects of an MPL on water and thermal management in a PEMFC. *Int J Energy Res*. 2019;43(1):274-296.

34. Kleemann J, Finsterwalder F, Tillmetz W. Characterisation of mechanical behaviour and coupled electrical properties of polymer electrolyte membrane fuel cell gas diffusion layers. *J Power Sources*. 2009;190(1):92-102.
35. Serincan MF, Pasaogullari U. Effect of gas diffusion layer anisotropy on mechanical stresses in a polymer electrolyte membrane. *J Power Sources*. 2011;196(3):1314-1320.
36. Qiu D, Yi P, Peng L, Lai X. Channel dimensional error effect of stamped bipolar plates on the characteristics of gas diffusion layer contact pressure for proton exchange membrane fuel cell stacks. *J Fuel Cell Sci Technol*. 2015;12(4).
37. Liang P, Qiu D, Peng L, Yi P, Lai X, Ni J. Structure failure of the sealing in the assembly process for proton exchange membrane fuel cells. *Int J Hydrogen Energy*. 2017;42(15):10217-10227.
38. Lykins CD, Mall S, Jain V. An evaluation of parameters for predicting fretting fatigue crack initiation. *Int J Fatigue*. 2000;22(8):703-716.
39. Shen J, Tu Z, Chan SH. Enhancement of mass transfer in a proton exchange membrane fuel cell with blockage in the flow channel. *Appl Therm Eng*. 2019;149:1408-1418.
40. Khorasany R, Singh Y, Alavijeh AS, Kjeang E, Wang G, Rajapakse R. Fatigue properties of catalyst coated membranes for fuel cells: ex-situ measurements supported by numerical simulations. *Int J Hydrogen Energy*. 2016;41(21):8992-9003.
41. Kakati BK, Deka D. Differences in physico-mechanical behaviors of resol (e) and novolac type phenolic resin based composite bipolar plate for proton exchange membrane (PEM) fuel cell. *Electrochim Acta*. 2007;52(25):7330-7336.
42. Nalwa HS. *Handbook of Advanced Electronic and Photonic Materials and Devices, Ten-Volume Set*. Vol 1. Cambridge, MA: Academic Press; 2000.
43. Ince A, Glinka G. A modification of Morrow and Smith–Watson–Topper mean stress correction models. *Fatigue Fract Eng Mater Struct*. 2011;34(11):854-867.
44. Peng L, Lai X, Hu P, Ni J. Flow channel shape optimum design for hydroformed metal bipolar plate in PEM fuel cell. *J Power Sources*. 2008;178(1):223-230.

How to cite this article: Liu W, Qiu D, Peng L, Yi P, Lai X. Mechanical degradation of proton exchange membrane during assembly and running processes in proton exchange membrane fuel cells with metallic bipolar plates. *Int J Energy Res*. 2020;44:8622–8634. https://doi.org/10.1002/er.5550